Asian Journal of Chemistry; Vol. 24, No. 8 (2012), 3571-3578

ASIAN JOURNAL OF CHEMISTRY

www.asianjournalofchemistry.co.in

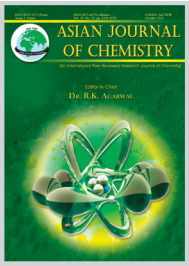

Computational Fluid Dynamics Studies of Hydrodynamic Parameters in a Two-Dimensional Conical Spouted Bed

BEHZAD SAEEDI RAZAVI[1] and SEYYED HOSSEIN HOSSEINI[2,*]

[1]Institute of Standard and Industrial Research of Iran, Khorassan Razavi 918583-7733, Iran
[2]Department of Chemical Engineering, Faculty of Engineering, University of Ilam, Ilam 69315-516, Iran

*Corresponding author: E-mail: s.h.hosseini@mail.ilam.ac.ir

(*Received*: 9 August 2011; *Accepted*: 19 March 2012) AJC-11193

Hydrodynamics behaviour of a pseudo 2D conical spouted bed was studied by computational fluid dynamics code MFIX. Simulations were done in the symmetery two-dimensional frameworks using an Eulerian-Eulerian approach incorporating the kinetic theory of granular flows. Incoherent and steady spouting were analyzed and several hydrodynamic parameters were evaluated. Some parameters that influence the incoherent and steady spouting were investigated by the model. The validated model showed that nozzle diameter and inlet width are the important parameters on the hydrodynamics of the conical spouted beds. The simulation results showed that the computational fluid dynamics can be used as an effective tool to provide information on the details of particles behaviour in the conical spouted beds.

Key Words: Conocal spouted bed, Hydrodynamics, Computational fluid dynamics, Two-dimension.

INTRODUCTION

Spouted beds, are widely aused in various physical operations such as drying, coating and granulation. Besides the physical application, these beds possess certain structural and flow characteristics that are very desirable for some chemical reaction systems. Consequently, increasing attention has been paid to the application of spouted beds as chemical reactors, including as catalytic partial oxidation, catalytic oxidative coupling reactors, catalytic polymerization reactors and pyrolysis reactors.

Due to the formation of strong solid circulations and high gas-solid contact in the conical spouted bed, this system has found wide applications in many chemical processes. In order to make more effective use of conical spouted beds in industrial applications, an improved theoretical understanding of conical spouted bed hydrodynamics is needed. Computational fluid dynamics (CFD) has now emerged as an effective tool for investigation of spouted bed hydrodynamics.

Several aspects of spouted beds hydrodynamics have been studied by the researchers. Huilin *et al.*[1,2] presented the results of their two-fluid model simulations for a conical spouted bed based on constant viscosity model. Wang *et al.*[3] simulated the axial and radial distributions of static pressures and vertical particle velocity distributions in conical spouted beds using the commercial computational fluid dynamics package Fluent. They showed that the introduction of a source term to modify the gravity effect in the annulus region is required for proper predictions of the flow.

Several researchers noted the importance of the expression for the drag functions used in simulation of gas-solid flows. Hosseini *et al.*[4] showed that various drag models should be investigated for different types of gas distributors or when an internal slotted draft tube is present. Du *et al.*[5] studied the effect of different correlations for the exchange coefficients and suggested that the Gidaspow drag model was the best choice in simulation of cylindrical spouted beds. Using the MFIX code, Hosseini *et al.*[6] studied the effects of different drag models on the simulation results of a cylindrical spouted bed with a non-porous draft tube containing a binary mixture of particles and found that Wen-Yu's drag function was most appropriate.

In addition to the gravity and drag forces, several researchers have shown that frictional stresses play an important role for the modeling of cylindrical spouted beds[2,7].

Zhong *et al.*[8] and Zhao *et al.*[9] simulated the hydrodynamics of a 2D spout-fluid bed using the DEM technique. The latter work reported the distribution of drag forces on the particles and particle velocity profiles in the bed.

In this study, the gas-solid flows in conical spouted beds were studied using an Eulerian-Eulerian two-fluid model embedded in computational fluid dynamics code MFIX. The circulating flow patterns in the bed and the hydrodynamic

properties of the solid and the gas phases were evaluated. Effects of bed heights and the superficial gas velocity as well as the conical base angle on the vertical particle velocities along the axis and stability of spouting were investigated. The simulation results for the conical spouted bed were compared with the experimental data and the results for the cylindrical spouted beds and discussed. Influence of some design parameters such as nozzle diameter and inlet width were studied on the hydrodynamics of a conical spouted bed by the computational fluid dynamics model.

EXPERIMENTAL

Model description: The Eulerian-Eulerian multiphase model that treats the gas and solid phases as interpenetrating continua was used in this study. To describe the particulate phase stress in the Eulerian-Eulerian approach, the kinetic theory of granular flow (KTGF) was used.

Continuity equation for phase k (k = g for gas or s for solid phase):

$$\frac{\partial}{\partial t}(\alpha_k \rho_k) + \frac{\partial}{\partial x_i}(\alpha_k \rho_k u_{ki}) = 0 \quad (1)$$

Momentum equations for solid phase:

$$\frac{\partial}{\partial t}(\alpha_s \rho_s u_{si}) + \frac{\partial}{\partial x_j}(\alpha_s \rho_s u_{sj} u_{si}) = -\alpha_s \frac{\partial P_g}{\partial x_i} + \frac{\partial \tau_{sij}}{\partial x_j} + I_{gsi} + \alpha_s \rho_s g_i \quad (2)$$

Momentum equations for gas phase:

$$\frac{\partial}{\partial t}(\alpha_g \rho_g u_{gi}) + \frac{\partial}{\partial x_j}(\alpha_g \rho_g u_{gj} u_{gi}) = -\alpha_g \frac{\partial P_g}{\partial x_i} + \frac{\partial \tau_{gij}}{\partial x_j} + I_{gsi} + \alpha_g \rho_g g_i \quad (3)$$

The expression for the drag is given as:

$$I_{gsi} = \beta_{gs}(u_{gi} - u_{si}) \quad (4)$$

The drag force acting on a particle in fluid-solid systems was modeled by:

$$\beta_{gs} = \frac{3}{4} C_D \frac{\rho_g \alpha_s}{d_s} |u_g - u_g| \alpha_g^{-1.65},\ C_D = \left(0.63 + \frac{4.8}{\sqrt{Re_s}}\right)^2 \quad (5)$$

Solid stresses in eqn. (2) are given by:

$$\tau_{sij} = (-P_s + \eta \mu_b \frac{\partial u_{si}}{\partial x_i})\delta_{ij} + 2\mu_s S_{sij} \quad (6)$$

where, the devitoric part of the deformation rate tensor is given as:

$$S_{sij} = \frac{1}{2}(\frac{\partial u_{si}}{\partial x_j} + \frac{\partial u_{sj}}{\partial x_i}) - \frac{1}{3}\frac{\partial u_{si}}{\partial x_i} \quad (7)$$

The expression for solid pressure is given as:

$$P_s = \alpha_s \rho_s \Theta_s [1 + 4\eta \alpha_s g_0] \quad (8)$$

The solids viscosity is given as:

$$\mu_s = (\frac{2+\alpha}{3})\left[\frac{\mu_s^*}{g_0 \eta(2-\eta)}(1 + \frac{8}{5}\eta \alpha_s g_0) \times (1 + \frac{8}{5}\eta(3\eta - 2(\alpha_s g_s) + \frac{3}{5}\eta \mu_b\right] \quad (9)$$

where

$$\mu_s^* = \frac{\rho_s \alpha_s g_0 \Theta_s \mu'}{\rho_s \alpha_s g_0 \Theta_s + (2\beta_{gs}\mu' / \rho_s \alpha_s}, \mu' = \frac{5}{96}\rho_s d_s \sqrt{\pi \Theta_s}, \mu_b = \frac{256}{5\pi}\mu' \alpha_s^2 g_0 \quad (10)$$

Solid conductivity of granular energy is given as:

$$\kappa_s = \left(\frac{\kappa_s^*}{g_0}\right)\left[\left(1 + \frac{12}{5}\eta \alpha_s g_0\right)\left(1 + \frac{12}{5}\eta^2(4\eta - 3(\alpha_s + g_0)\right) + \frac{64}{25\pi}(41 - 33\eta^2(\alpha_s g_0)^2\right],$$

$$\kappa_s^* = \frac{\rho_s \alpha_s g_0 \Theta_s \kappa}{\rho_s \alpha_s g_0 \Theta_s + \left(\frac{6\beta_{gs}\kappa}{5\rho_s \alpha_s}\right)},\ \kappa = \frac{75\rho_s d_s \sqrt{\pi \Theta_s}}{48\eta(41 - 33\eta)} \quad (11)$$

The formulation of Carnahan and Starling is used for the radial distribution function. The transport equation for granular temperature (kinetic energy) Θ is given as:

$$\frac{3}{2}\alpha_s \rho_s [\frac{\partial \Theta_s}{\partial t} + u_{sj}\frac{\partial \Theta_s}{\partial x_j}] = \frac{\partial}{\partial x_j}(\alpha_s \rho_s \kappa_s \frac{\partial \Theta_s}{\partial_i}) + \alpha_s \rho_s \tau_{sij}\frac{\partial u_{si}}{\partial x_j} + \Pi_s - \alpha_s \rho_s J_s \quad (12)$$

where, the collisional dissipation is given by

$$J_s = \frac{48}{\sqrt{\pi}}\eta(1-\eta)\frac{\alpha_s g_0}{d_s}\Theta_s^{3/2}, \eta = \frac{1+e}{2} \quad (13)$$

and the exchange terms are given by:

$$\Pi_s = -3\beta_{gs}\Theta_s + \frac{81\alpha_s \mu_g^2 |u_g - u_s|^2}{g_s d_s^3 \rho_s \sqrt{\pi \Theta_s}} \quad (14)$$

Syamlal *et al.*[10] suggested a more refined model which is activated when the solids volume fraction exceeds the maximum packing limit (α_s^{max}). That is,

$$P_f = P_c = \begin{cases} 10^{25}(\alpha_s - \alpha_s^{max})^{10}, \alpha_s > \alpha_s^{max} \\ 0 \qquad\qquad \alpha_s \le \alpha_s^{max} \end{cases} \quad (15)$$

$$\mu_f = \begin{cases} \min\left(\frac{P_c \sin(\phi)}{\sqrt{4I_{2D}}}, \mu_m^{max}\right), \alpha_s > \alpha_s^{max} \\ 0 \qquad\qquad \alpha_s \le \alpha_s^{max} \end{cases} \quad (16)$$

where μ_m^{max} = 1000 P.

$$I_{2D} = \frac{1}{6}[(D_{s11} - D_{s22})^2 + (D_{s22} - D_{s33})^2 + (D_{s33} - D_{s11})^2] + D_{s12}^2 + D_{s23}^2 + D_{s31}^2 \quad (17)$$

and $D_{sij} = \frac{1}{2}(\frac{\partial u_{si}}{\partial x_j} + \frac{\partial u_{sj}}{\partial x_i})$

The frictional stress model of Srivastava and Sundaresan[11] influences the flow behaviour at solid volume fractions below maximum packing:

$$P_c = \begin{cases} 10^{25}(\alpha_s - \alpha_s^{max})^{10} & \alpha_s > \alpha_s^{max} \\ Fr\frac{(\alpha_s - \alpha_s^{min})^r}{(\alpha_s^{max} - \alpha_s)^s} & \alpha_s^{max} \ge \alpha, > \alpha_s^{min} \\ 0 & \alpha_s \le \alpha_s^{min} \end{cases} \quad (18)$$

$$P_f = P_c\left(1 - \frac{\nabla \cdot u_s}{n\sqrt{2}\sin\phi\sqrt{S:S + \Theta_s / d_s^2}}\right)^{n-1} \quad (19)$$

$$\mu_f = \frac{\sqrt{2}\sin\phi P_f}{\left(\sqrt{S:S + \Theta_s / d_s^2}\right)}\left(n - (n-1)\left(\frac{P_f}{P_c}\right)^{\frac{1}{n-1}}\right) \quad (20)$$

The value of ϕ is taken to be 28.5º for glass. In this study, the effect of minimum frictional solids volume fraction is investigated. Fr, r and s are empirical material constants, which are taken to be, respectively, 0.5, 2.0 and 5. The coefficient n is selected depending on whether the granular assembly experiences a dilatation or compaction:

$$n = \begin{cases} \dfrac{\sqrt{3}}{2\sin\phi} & \nabla \cdot u_m \geq 0 \\ 1.03 & \nabla \cdot u_m < 0 \end{cases} \quad (21)$$

$$\mu_f^{bulk} = -\frac{2}{3}\mu_f \quad (22)$$

Model solution procedure: In the present study, simulations are performed for the experimental condition of Liu *et al.*[12] for a two-dimensional conical spouted bed. The corresponding configuration of the setup and the experimental conditions are listed in Table-1.

TABLE-1
EXPERIMENTAL CONDITION OF THE 2D CONICAL SPOUTED BED[12]

Parameter	Unit	Values
Particle diameter (d_s)	cm	0.2
Particle density (ρ_s)	g/cm^3	2.38
Superficial gas velocity (U_g)	cm/s	152-195
Stagnant bed height (H_b)	cm	7.5, 10
Slot width, nozzle diameter (λ)	cm	0.9
Inlet width (D_i)	cm	1.9
Column width (α)	cm	15.2
Column thickness (β)	cm	1.5
Inclined angle (θ)	o	60

The set of non-linear equations is linearized using a modified version of the SIMPLE algorithm using the void fraction and gas pressure correction equations.

The adaptive time step in the range of 10^{-5}-10^{-2} is used. The gas was air and the solids were glass beads. Computational fluid dynamics code MFIX, was used to simulate the hydrodynamics of a conical spouted bed. The system is assumed to be symmetrical. A convergence criterion of 10^{-3} for each scaled residual component is fixed for the relative error between two iterations. The boundary conditions are as follow: 1. At the bottom of the bed, the gas injects only in the axial direction, so the inlet gas velocity is used; 2. The pressure boundary condition is set at atmospheric on the top of the freeboard; 3. On the bed wall, a no slip boundary condition is assumed for the both phases; 4. The axis is initialized as a free-slip wall.

Computational grids: A two-dimensional symmetry model in Cartesian framework is used. The mesh size is taken to be 2 mm near the lateral bed wall and 1.18 mm at the center of the spout section and varied along the axial direction of the bed from 2.0 mm to 9.8 mm. The structure of the grids in the computational domain is illustrated in Fig. 1.

First, the grid sensitivity was tested by evaluating the computational fluid dynamics results for three grid sizes. As can be seen in Fig. 2, the coarse grid (24 × 60) gives a low axial particle velocity along the axial. The intermediate grid (45 × 70) and fine grid (50 × 120), however, lead to the same variations along the axial direction. Therefore, the fine grid (50 × 120) was used in the rest of the simulations.

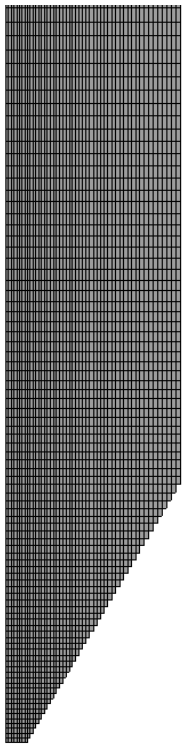

Fig. 1. Computational domain

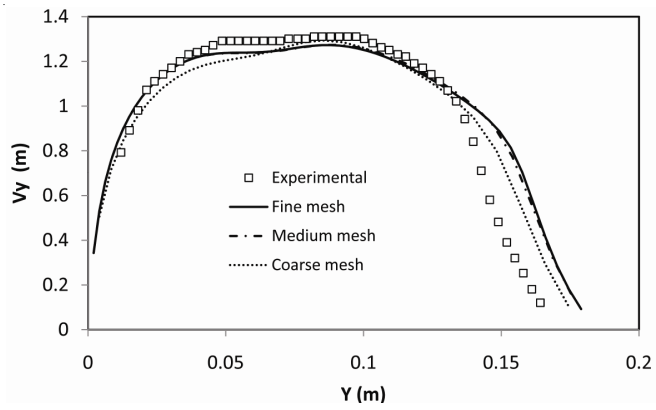

Fig. 2. Computed and measured vertical velocities of particles along the axis to investigate mesh independency

RESULTS AND DISCUSSION

Influences of coefficient of restitution: It was observed from the computational results that as the restitution coefficient increases (collision are more elastic), the fountain height and vertical particle velocity along the axis decrease. The decrease in dissipation rate causes the granular temperature to increase, leading to an increase in the solid shear viscosity and diffusion, resulting in lower gas volume fraction. In addition, increasing the restitution coefficient, leads to the increase of the stability of the spout. In summary, the restitution coefficient significantly influences the stability of spout and particle flow parameters. Simulations were carried out for restitution coefficient of 0.8, 0.9 and 0.97 for a constant value of transition point (α_s^{min}). Computational fluid dynamics code (MFIX), showed that the

most appropriate coefficient of restitution by considering drag function presented in eqn. (5) for predicting axial particle velocity along the axis and fountain height is 0.8. Therefore, coefficient of restitution of 0.8 was used in the rest of the simulations.

Frictional stresses models: When the particle concentration is high, the behaviour of the granular flow cannot be adequately described by kinetic theory. This is because at high solids volume fractions continuous contacts occur among the particles. Inclusion of the frictional stress is important and is needed for modeling the gas-fluidization systems with the very dense regions.

The frictional stress models of Syamlal *et al.*[10] and Srivastava and Sundaresan[11] with various values of minimum concentration for the transition point (α_s^{min}) are used in the simulations to examine the effect of the frictional stress on the computational fluid dynamics simulation. For U_g = 1.95 and H_b = 10 cm, the vertical particle velocities along the axis as predicted by the kinetic theory model with and without frictional stresses are compared with the experimental data in Fig. 3. The kinetic theory of the granular flow without frictional stresses overpredicts the vertical particle velocities in the spout and fountain zones.

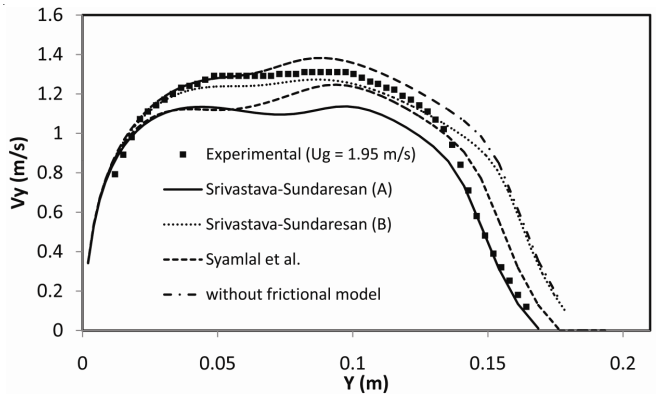

Fig. 3. Computed profiles of vertical velocities of particles with different frictional stresses models and measured one along the axis at U_g = 1.95 m/s and H_b = 10 cm

A sensitivity analysis of the simulation results for the Srivastava and Sundaresan frictional stress model is performed by changing the minimum value of the particulate phase fraction at which the frictional stress model becomes effective. It is seen that the frictional stress model of Srivastava and Sundaresan with α_s^{min} = 0.5 leads to a significant under-prediction of the vertical particle velocity in the spout region (model (A) in Fig. 3), while this model with $\alpha_s^{min} = \alpha_s^{max} = 0.6$ predicts the proper trend in the spout region (model (B) in Fig. 3). Reducing the value of minimum concentration implies inclusion of the frictional stresses for the particulate phase for lower concentrations.

The solid volume fraction contour shown in Fig. 4, is obtained for both models of A ($\alpha_s^{min} = 0.5$) and B ($\alpha_s^{min} = 0.6$). It is found that at a low value of α_s^{min} steady spouting is reached.

The minimum value of the particulate phase fraction of 0.5 for transition that first time was suggested empirically by Johnson and Jackson[13], have been used by many researchers for simulations of dense gas-solid fluidization systems.

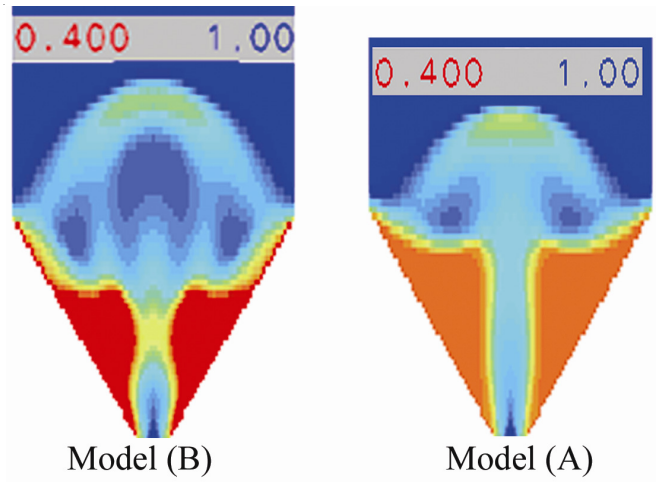

Fig. 4. Solid volume fraction contour for both models A and B

In summary, Figs. 3 and 4 show that the frictional stress can significantly affect the hydrodynamics of the spout, so its influence must be included in the simulation of the conical spouted bed. Furthermore, the combined kinetic-friction model allows for accurate prediction of the flow behaviour. Another conclusion is the transition solid volume fraction noticeably affects the behaviour of the granular temperature in the bed and the associated hydrodynamics of the conical spouted beds.

Spout state: Steady spouting in the cylindrical spouted beds has been found in the numerical and experimental results of many researchers. For instance, cylindrical spouted bed operated by Ishikura *et al.*[14] has been simulated here to observe state of spout in this type of the spouted beds. Fig. 5 shows the gas volume fraction after 5s in the cylindrical spouted bed of Ishikura *et al.* for $U_g = 1.1U_s$. As can be seen in the figure the spout shape is not change with time and steady spouting is established. This behaviour has been found by several researchers[5,6,15].

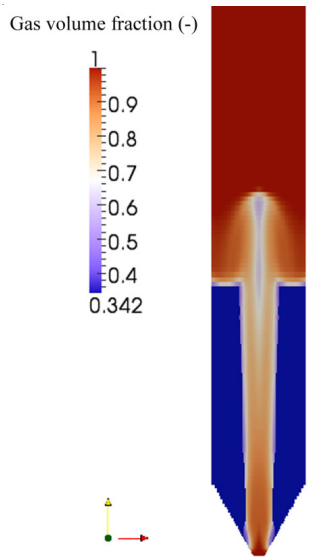

Fig. 5. Computed gas volume fraction for the Ishikura *et al.*[14] cylindrical spouted bed at $U_g = 1.1U_s$

Incoherent spouting was first reported by Dogan *et al.*[16] in a thin-slot, rectangular spouted bed. Liu *et al.*[12] attributed

the incoherent spouting regime to periodic altering of the spout shape and the periodic movement of particles in the annulus region.

Fig. 6 shows snapshots of contour plots of solid volume fraction for U_g = 1.95 m/s and H_b = 10 cm. Unlike the previous works, Fig. 6 shows that the spout geometry and the resulting fountain height are not steady and change periodically with time. Good agreement between the numerical simulations and the experimental findings of Liu *et al.*[12] is observed. A close examination of Fig. 6 shows that, unlike the bed surface in cylindrical spouted beds (see Fig. 5), the surface is not flat but concave. This trend of bed surface shape is apparent in both experimental and numerical results.

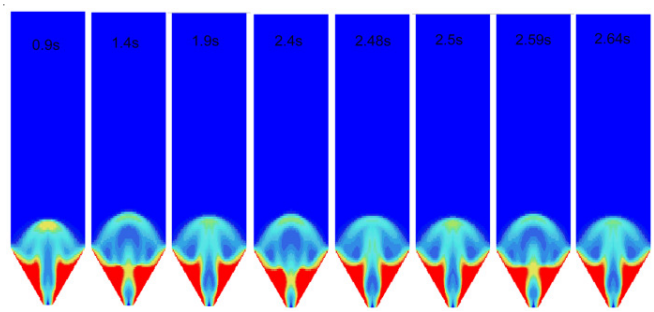

Fig. 6. Instantaneous concentrations of particles at U_g = 1.95 and H_b = 10 cm

The incoherent spouting is tied to the bed pressure drop fluctuations[17]. To obtain a better understanding of the periodicity of the particle flow in the annulus region, the fluctuation of bed pressure drop is evaluated. The corresponding power spectrum of the pressure fluctuation at x = 3.8 cm and y = 7 cm in the annulus was evaluated by the model (Fig. 7).

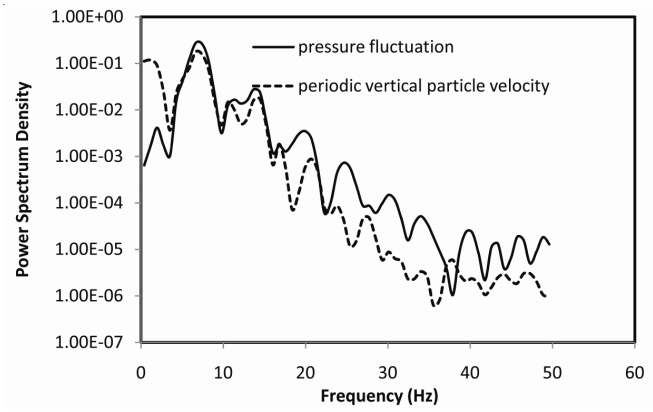

Fig. 7. Computed power spectrum density of the pressure fluctuation and periodic vertical particle velocity at x = 3.8 cm and y = 7 cm in the annulus

The dominant spectral peaks for the experiment and the model are, respectively, at 6.47 and 6.64 Hz. These frequencies are approximately equal to the dominant frequency of F_d = 6.41 Hz for the periodic motion of particles in the annulus region.

Static bed height: Fig. 8 shows the longitudinal profiles of vertical particle velocity, Vy, along the spout axis for superficial gas velocities of U_g = 1.58, 1.77 and 1.95 m/s and stagnant bed height of H_b = 10.0 cm. For these gas velocities, the model predicts proper results in the spout while it overpredicts the particle vertical velocities in the fountain region, which leads to the overprediction of the fountain heights. To predict the fountain accurately, the predicted particle vertical velocities need to be fitted to the experimental data. To reduce the fountain height, the frictional stresses should be evaluated properly (Figs. 3 and 4). However, this additional effort requires the development of a more suitable frictional stresses model and is left for a future work.

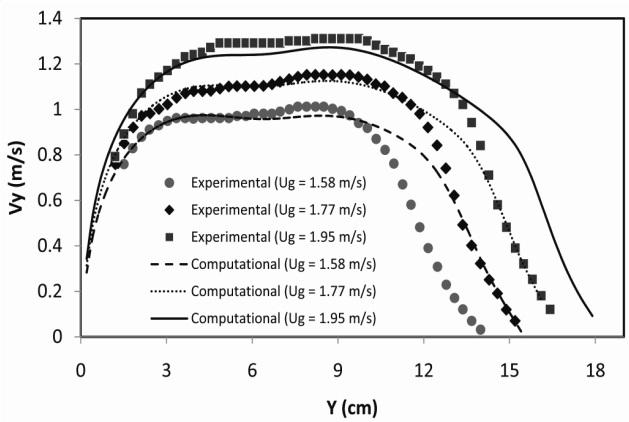

Fig. 8. Computed and measured profiles of vertical particle velocities along the spout axis at different superficial gas velocities and H_b = 10 cm

Fig. 9 shows the longitudinal profiles of vertical particle velocity, Vy, along the spout axis for different superficial gas velocities U_g = 1.52, 1.71 and 1.89 m/s and a stagnant bed height of H_b = 7.5 cm. The simulated results are also compared with the experimental data. It is seen that the particles are quickly accelerated near the inlet zone and then the particle velocity profile stays roughly flat. This figure shows the particle acceleration in the upper spout region is insignificant. Vertical particle velocity reaches its maximum value near the spout end and then decelerates gradually in the fountain region. This behaviour was discussed at length in the early work of Liu *et al.*[12].

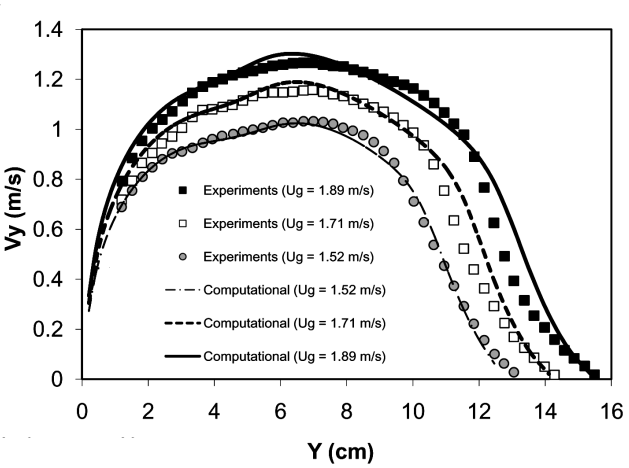

Fig. 9. Computed and measured profiles of vertical particle velocities along the spout axis at different superficial gas velocities and Hb = 7.5 cm

Fig. 9 shows the influence of static bed height on the vertical particle velocity along the axis. Comparing Fig. 9 to Fig. 8, it is seen that for H_b = 10.0 cm, the flat peak zone of the

particle vertical velocity is relatively short. That is, for a constant superficial gas velocity greater than the minimum spouting gas velocity, a decrease in the static bed height decreases the flat region of the particle velocity profile. For a fixed superficial velocity but different bed heights, the acceleration of the particles in the lower part of the spout is quite similar. As shown in Figs. 8 and 9 the peak velocities of these two cases for the same value of U_g are very close.

As can be seen from Figs. 8 and 9, the predicted vertical particle velocity in the fountain region for H = 10 cm is not as satisfactory as that for H = 7.5 cm. When the static bed height is H = 10 cm, the bed includes a larger amount of particles than does the bed with H = 7.5 cm, so the frictional stresses are more significant compared to the case for H = 7.5 cm. The loss of computational accuracy for the bed with H = 10 cm suggest the increasing importance of frictional stresses. For a larger bed, the influence of frictional stresses increases; therefore, a more suitable frictional stress model is needed to improve the model predictions for larger H. The sensitivity of the model prediction to the frictional stress was shown in Figs. 3 and 4 for the bed with static bed height of H = 10 cm.

The predicted profile of vertical particle velocity along the spout axis for the Ishikura *et al*. cylindrical spouted bed at $U_g = 1.1Us$ is shown in Fig. 10. From Figs. 8-10 it is found that the particle vertical velocity profiles along the axis in the conical spouted beds greatly differ from those observed in the cylindrical spouted beds. It is observed in Fig. 10 that the particles in the cylindrical spouted bed are rapidly accelerated to their maximum velocity at a height near the inlet zone; after that particles gradually decelerate and their velocity sharply decreases to zero in the fountain region. This behaviour is also observed by the researchers[5].

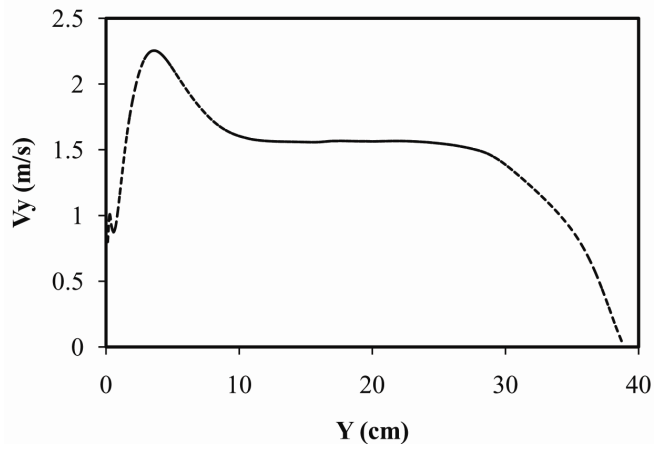

Fig. 10. Computed profiles of vertical particle velocity along the spout axis for the Ishikura *et al*.[14] cylindrical spouted bed at $U_g = 1.1Us$

Effect of spout nozzle diameter on vertical particle velocities: The comparisons of vertical particle velocities profiles along the spout axis for two spout nozzles of 0.6 and 0.9 cm are shown in Fig. 11 at $U_g = 1.95$ m/s and $H_b = 10$ cm. At a given spouting gas velocity, the vertical particle velocities profiles along the spout axis decreases with the decreasing of spout nozzle diameter, which due to the decreasing of spout gas momentum. According to the Turner's theory, the jet momentum flow rate can be expressed as:

$$M = \frac{\pi}{4} d_s^2 \rho_g u_s \quad (23)$$

Therefore, by increasing spouting gas velocity, the jet momentum flow rate increases, which leads to the increasing of the vertical particle velocities profiles along the spout axis.

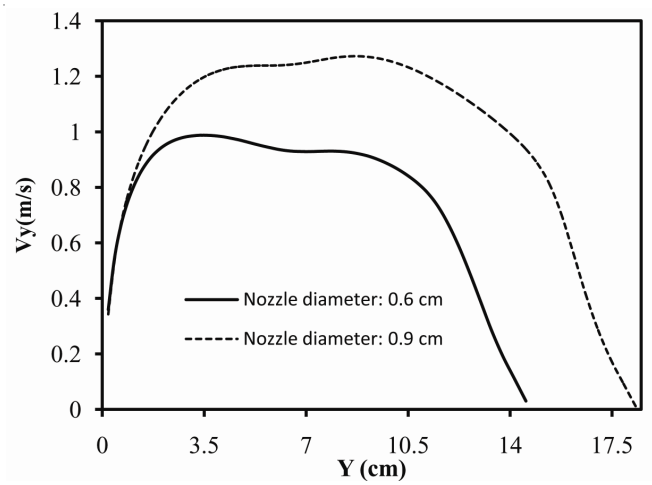

Fig. 11. Computed profiles of vertical particle velocities along the spout axis for different nozzle diameters at $U_g = 1.95$ m/s and $H_b = 10$ cm

Besides increasing the vertical particle velocities profiles along the spout axis, fountain heigh decreases with decreasing nozzle diameter or decreasing of spout gas momentum. Zhong *et al*.[18] showed that the jet penetration depth increases with increasing spouting gas velocity and spout nozzle diameter in the 2D conventional spouted bed.

Effect of inlet width, D_i: No experimental data are available in the literature to study the effect of inlet width on hydrodynamics of conical spouted beds. Thus, the adopted model is used in the new design. Therefore, for the same content of the solid particles in the cone section of the bed and $U_g = 1.95$ m/s, effect of inlet width (D_i) on the solid behaviour is investigated. For this purpose three inlet widths of 0.9, 1.9 and 2.62 cm for the bed with nozzle diameter of 0.9 cm are selected.

Fig. 12 indicates the vertical particle velocities profiles along the spout axis for different inlet widths. As can be seen in the figure with increasing inlet width, solid particle velocity increases till Y = 13 cm and after that inverse behaviour is observed. The differences of axial solid velocity along the central line of the bed for different inlet widths are considerable. Thus, the inlet width influences on the hydrodynamics parameters of the bed.

Fig. 13 shows the predicted time-averaged gas volume fraction and solid particle velocity vectors for the bed with different inlet widths. The solid concentration in the cone section of the bed for inlet width of 2.62 cm is higher than the bed with inlet width of 0.9 cm. In addition, the qualitative behaviour of the particles, particle circulations, for both inlet widths are similar.

As can be seen in the figure, particle velocity in the spout is higher than that in the annulus. The rain of particles spreads in the wide fountain periphery. Particles from the spout move downwards in the fountain and then fall into the annulus. Near the entrance region surrounding the gas inlet, the particles are

transported from the annulus to the spout and are entrained in the gas, then move upward within the spout region due to the gas drag force, rise into the fountain and finally fall down into the annulus. As particles fall into the annulus, the cycle repeats itself, which leads to the particle circulation in the conical spouted beds. In the annulus, the magnitude of particle velocity is low and the solid concentration is high, because in this region the particle gravity is balanced by the particle contact forces. These interactions result in lower velocity of downward moving particles.

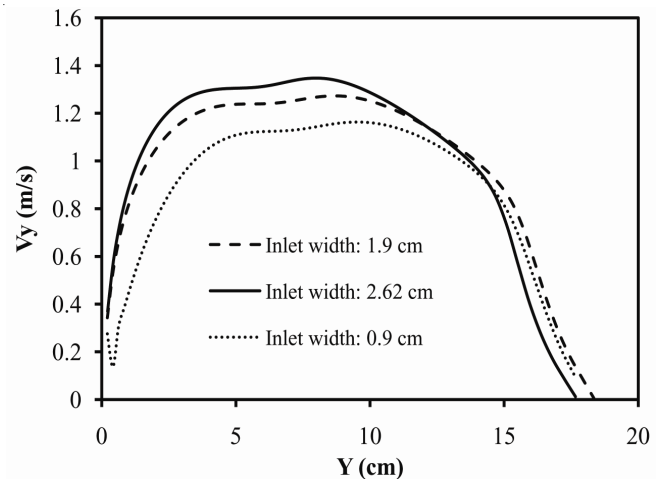

Fig. 12. Computed profiles of vertical particle velocities along the spout axis for different inlet widths at U_g = 1.95 m/s and same content of the particles

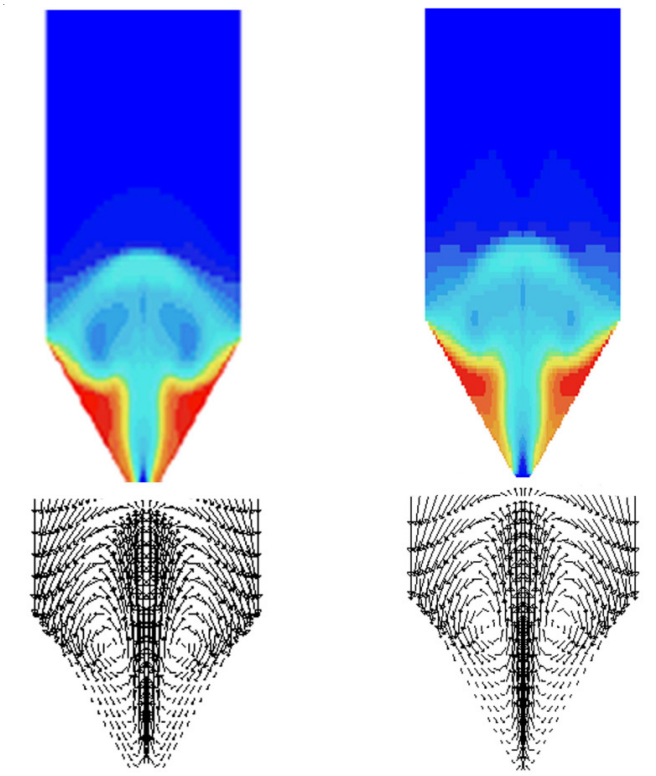

Fig. 13. Computed results of time-averaged gas volume fraction and solid particle velocity vectors for different inlet widths at U_g = 1.95 m/s and same content of the particles

Conclusion

In this study, a two-dimensional conical spouted bed was studied by an Eulerian-Eulerian approach embedded in the open source code MFIX. The presented results highlight the importance of frictional stresses in the simulations of conical spouted beds. Different frictional models were studied and a range of transient points for inclusion of frictional stresses (α_s^{min}) was tested. The simulation showed the expected flat profile for particle vertical velocity along the axis of the conical spouted bed. The effect of stagnant bed height on the profile of particle vertical velocity along the axis was also investigated. It was found that with increases in the static bed height, the length of the flat profile of the particle vertical velocity along the axis increases for the conical spouted bed. Several aspects of the hydrodynamics behaviour of the conical spouted bed were compared with the corresponding results in the cylindrical spouted beds with conical base and the disagreements were noted. The periodic circulation pattern of particle motion in the annulus was also studied and the incoherent spouting was discussed. It was found that, frictional stresses models have an important role in creation of state of the spout.

Effects of two design parameters of nozzle diameter and inlet width were also investigated by the computational fluid dynamics code MFIX. At a constant gas velocity, with increasing the nozzle diameter, particle vertical velocity along the spout axis and fountain heigh increases. In addition, inlet width has a significant effect on the hydrodynamics of conical spouted beds that it should be studied and designed for each conical spouted bed.

Nomenclatures

α	Volume fraction, [-].
α_{mf}	Gas volume fraction at minimum fluidization, [-].
α_s^{max}	Maximum solid volume fraction, [-].
α_s^{min}	Solid fraction at the transition point, [-].
β_{gs}	Gas/solid momentum exchange coefficient, [kg/m^{3}s]
Θ_s	Granular temperature, [m^2/s^2].
κ_s	Solid conductivity of granular energy, [W/m K].
μ	Shear viscosity, [kg/m s].
Π_s	Granular temperature exchange term, [kg/ms^3].
ρ_i	Density, [kg/m^3].
τ_{kij}	Stress tensor of phase k, [Pa].
ϕ	Angle of internal friction, [deg].
ϕ_p	Specularity coefficient, [-].
d_s	Particle mean diameter, [m].
D_{sij}	Rate of strain tensor, solid phase, [s^{-1}].
e	Restitution coefficient, [-].
g_i	Acceleration due to gravity, [m/s^2].
g_0	Radial distribution coefficient, [-].
H_b	Static bed height, [m].
I_{gsi}	Momentum transfer from fluid phase to solid phase, [N/m^3].
J_s	Collisional dissipation, [m^2/s^3].
P	Pressure, [Pa].
P_c	Critical pressure in solid phase, [Pa].
P_f	Frictional pressure in solid phase, [Pa].
Re_s	Particle Reynolds number, [-].
S_{sij}	Deviatoric part of the rate-of-strain, [s^{-1}].
S	Deviatoric part of the rate-of-strain tensor, [s^{-1}].

t Time, [s].
u Velocity vector, [m/s].
y Coordinate, [m].

Sub/superscripts

f Friction
s Solid phase.
g Gas phase.
c Critical

REFERENCES

1. L. Huilin, S. Yongli, L. Yang, H. Yurong and J. Bouillard, *Chem. Eng. Res. Des.*, **79**, 593 (2001).
2. L. Huilin, H. Yurong, L. Wentie, D. Jianmin, D. Gidaspow and J. Bouillard, *Chem. Eng. Sci.*, **59**, 865 (2004).
3. Z.G. Wang, H.T. Bi and C.J. Lim, *China Particuol.*, **4**, 194 (2006).
4. S.H. Hosseini, G. Ahmadi, R. Rahimi, M. Zivdar and M.N. Esfahany, *Powder Technol.*, **200**, 202 (2010).
5. W. Du, X.J. Bao, J. Xu and W.S. Wei, *Chem. Eng. Sci.*, **61**, 1401 (2006).
6. S.H. Hosseini, M. Zivdar and R. Rahimi, *Chem. Eng. Proc.*, **48**, 1539 (2009).
7. W. Shuyan, L. Xiang, L. Huilin, Y. Long, S. Dan, H. Yurong and D. Yonglong, *Powder Technol.*, **196**, 184 (2009).
8. W. Zhong, Y. Xiong, Z. Yuan and M. Zhang, *Chem. Eng. Sci.*, **61**, 1571 (2006).
9. X.-L. Zhao, S.-Q. Li, G.-Q. Liu, Q. Yao and J.-S. Marshall, *Powder Technol.*, **184**, 205 (2008).
10. M. Syamlal, W. Rogers and T.J. O'Brien, MFIX Documentation: Theory and Guide. Technical Report DOE/METC-94/1004 (DE9400087), Morgantown Energy Technology Centre, Morgantown, West Virginia (1993).
11. A. Srivastava and S. Sundaresan, *Powder Technol.*, **129**, 72 (2003).
12. G.-Q. Liu, S.-Q. Li, X.-L. Zhao and Q. Yao, *Chem. Eng. Sci.*, **63**, 1131 (2008).
13. P.C. Johnson and R. Jackson, *J. Fluid Mech.*, **176**, 67 (1987).
14. T. Ishikura, H. Nagashima and M. Ide, *Powder Technol*., **131**, 56 (2003).
15. W. Du, X.J. Bao, J. Xu and W.S. Wei, *Chem. Eng. Sci.*, **61**, 4558 (2006).
16. O.M. Dogan, L.A.P. Freitas, C.J. Lim, J.R. Grace and B. Luo, *Chem. Eng. Commun.*, **181**, 225 (2000).
17. J. Xu, X. Bao, W. Wei, G. Shi, S. Shen, H.T. Bi, J.R. Grace and C.J. Lim, *Powder Technol.*, **140**, 141 (2004).
18. W. Zhong and M. Zhang, *Chem. Eng. Sci.*, **60**, 315 (2005).